AJNR

Morphologic Analysis of Normal Human Lumbar Dorsal Root Ganglion by 3D MR Imaging

J. Shen, H.-Y. Wang, J.-Y. Chen and B.-L. Liang

AJNR Am J Neuroradiol 2006, 27 (10) 2098-2103
http://www.ajnr.org/content/27/10/2098

ORIGINAL RESEARCH

Morphologic Analysis of Normal Human Lumbar Dorsal Root Ganglion by 3D MR Imaging

J. Shen
H.-Y. Wang
J.-Y. Chen
B.-L. Liang

BACKGROUND AND PURPOSE: The dorsal root ganglion (DRG) of the spinal nerve has been considered a key structure in the mechanism of low-back pain and radicular symptoms. The purpose of this study was to clarify the normal morphologic features and variations of the lumbar DRGs in a healthy population by using 3D MR imaging.

METHODS: 3D fast-field echo (FFE) with water selective excitation coronal MR images of lumbar spine obtained in 115 healthy volunteers were further reconstructed into a radial stack of 15 coronal images by using maximum intensity projection technique. The DRGs from L1 through L5 were assessed for the location, signal intensity, architecture, and dimensions.

RESULTS: Most DGRs were foraminal in location. Only 5.7% of the L5 DGRs were located intraspinally. The sizes of L1, L2, and L5 DRGs in men were larger than those in women ($P < .05$). The dimensions of the DRGs gradually increased from L1 to L5 ($P < .0001$). The biganglia (2 ganglial components) frequently occurred in the L4 and L3 DRGs, whereas the singular ganglion (1 ganglial component), in the L5 and L1 DRGs.

CONCLUSION: The normal anatomy and variants of the lumbar DRG could be better demonstrated by 3D MR imaging with water selective excitation technique. The relatively larger and more proximally located DRGs in the lower lumbar region may be more susceptible to compression. An appreciation of normal anatomy and variants of DRGs radiologically is helpful for the diagnosis and proper treatment for radiculopathy.

The dorsal root ganglion (DRG) is important when considering the mechanism of low-back pain and sciatica.[1] DRGs are highly sensitive to mechanical compression and closely related to abnormal sensations and pain in radiculopathy.[2] Previously, the DRG located proximally in the lumbar spine was suggested to be 1 of the causative factors of radicular symptoms in patients with lumbar disk herniation or spinal canal stenosis.[3] Moreover, in patients with extraforaminal lumbar disk herniation, the location of the DRG has been reported to influence the severity of the radicular symptoms.[4] Recently, results of an observational study showed beneficial effects of the lumbosacral percutaneous radio-frequency treatment of DRG in chronic back pain radiating to the leg, with success rates of up to 60%.[5] CT-guided periganglionic steroid injections were suggested as being an integral part of the management strategy for radicular pain resistant to medical treatment.[6] Therefore, thorough knowledge of the anatomy and variants of the DRGs is important not only for the correct diagnosis and understanding of pathologic anatomy in degenerative disorders but also for the refinement of proper interventional treatments.

There have been several anatomic studies of the lumbosacral DRG.[7-10] Most authors used either cadavers or symptomatic patients, with an invasive radiculogram or noninvasive MR imaging to study the anatomic details of the DRGs. However, normal radiologic anatomy of the DRGs in living humans has not been well explored. Only Hasegawa et al[10] investigated the morphology of the lumbosacral DRGs in 20 healthy male adults by using conventional coronal MR imaging. Because the DRGs normally lie obliquely within the superolateral portion of the lumbar intervertebral foramen, neither cross-sectional axial nor coronal MR imaging could provide a 3D view and thereby a comprehensive analysis of the DRGs.

The purpose of this study was to investigate the normal radiologic anatomy of the lumbar DRGs in the general population of healthy volunteers with a wide age range by using 3D coronal MR imaging and to provide important baseline anatomic information about the DRGs.

Methods

Subjects

The study protocol was approved in accordance with the recommendations of the Human Research Committee of our institution. One hundred twenty-two healthy volunteers who had no history of back pain or radiculopathy or spinal diseases or spinal surgery were recruited. After the procedure was fully explained, informed consent was obtained from all the volunteers. The age ranged from 15 to 75 years, with a mean age of 40.3 years. Six female adults were excluded from imaging analysis because of metallic artifacts from the intrauterine contraceptive device impeding evaluation of the DRGs, and 1 female adult was excluded because of lumbar scoliosis. Finally, the MR images of 115 volunteers (54 men, 61 women; age range, 15–75 years with a mean of 40 years) were analyzed.

MR Imaging

MR imaging was performed on a 1.5T whole-body unit (Intera, Philips Medical Systems, Best, the Netherlands) with a synergy spine coil with the patient in the supine position. Conventional fast spin-echo sagittal images were initially acquired for orientation. Then, 3D coronal fast-field echo (FFE) sequences with selective water excitation by using the principles of the selective excitation technique (Proset, see "Discussion") of the lumbar spine (L1 through L5), comprising a slab

Received October 20, 2005; accepted after revision February 1, 2006.

From the Department of Radiology (J.S., B.-L.L., J.-Y.C.), the Second Affiliated Hospital, Sun Yat-sen University, Guangdong, P.R.China; and the Department of Radiology (H.-Y.W.), Jiangsu Tumor Hospital, Jiangsu, P.R.China.

Please address correspondence to: Jun Shen, MD, Department of Radiology, the Second Affiliated Hospital, Sun Yat-sen University'107 Yanjiang West Rd, Guangzhou, 510120, Guangdong, P.R.China; e-mail: vencentsj@tom.com

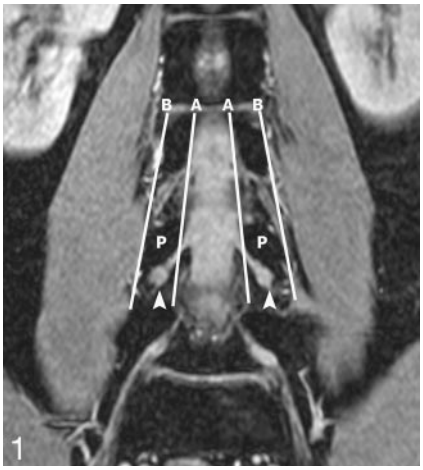

Fig 1. Determination of DRG position. The position of the DRG was determined on the original coronal FFE images. A and B are the lines respectively connecting the medial and lateral borders of the pedicles. If the midpoint of the DRG lies proximal to A, it is an intraspinal type; between A and B, a foraminal type; and distal to B, an extraforaminal type. In this 28-year-old volunteer, the L4 DRGs are the foraminal type (*arrowheads*). P indicates the L4 vertebral pedicles.

Fig 2. Lumbar DRGs on coronal MIP imaging. The reconstructed MIP image clearly depicts the DRGs of the spinal nerve bilaterally from L1 to L5, which demonstrates intermediate signal intensity (*arrowheads* indicate DRGs from L4 to L1; *arrows* indicate L5 DRGs).

of 40 contiguous images for each subject, were acquired with following acquisition parameters: 20-mm section thickness with 1-mm overlapping section gap; 28-cm field of view; 256 × 256 matrix; TR, 26.7 ms; TE, 18.3 ms; 8° flip angle; and 3 signal-intensity acquisitions. To obtain images of all the lumbar DRGs, we set the imaging plane to be parallel to the longitudinal axis of the lumbar spinal cord and centered on the level of the L3 vertebral body. Two perpendicular regional saturation slabs were added to suppress the signal intensity from the spinal vessels. The resultant whole-imaging slab had an anteroposterior thickness of 4 cm, which could fully cover the intervertebral foramina region from the posterior third vertebral body to the anterior third spinous process. The original coronal images were further reconstructed into a radial stack by using a maximum intensity projection (MIP) technique on the console. For 3D visualization of DRGs, the radial stack was set to rotate around the spinal cord with an interval of 12°. Finally, a series of 15 consecutive coronal MIP images were obtained.

Imaging Analysis

On the original coronal FFE images, the location of the DRGs was determined according to the previous method.[9] On the radial coronal MIP images, after all the DRGs were identified, we subsequently made the following morphometric evaluations on the plane where the DRG was maximally visualized: 1) The position of the DRG was determined by relating its midpoint to the intraspinal, foraminal, and extraforaminal regions. The intraspinal region was located medial to the medial border of the pedicle. The extraforaminal region is lateral to the lateral border of the pedicle, and the foraminal region was confined to the medial and lateral borders of the pedicle (Fig 1). 2) The signal intensity of the DRGs was determined as intermediate intensity or high intensity in comparison with the spinal cord at higher levels. The signal intensity of DRG was similar to, or obviously higher than, that of the spinal cord; it was considered as intermediate intensity and high intensity, respectively. 3) The dimensions of the DRGs, in terms of length, width, and width/length ratio were measured at the maximal visualization plane. The length was measured as the longitudinal distance between the proximal and distal ends of DRG along with the spinal nerve. The width was measured vertically at the midpoint perpendicular to the longitudinal axis of DRG. 4) The architecture of DRGs was classified into 3 types according to their composition as singular ganglion, biganglia, and triganglia. The singular ganglion had only 1 ganglion (1 component). The biganglia type had 2 seemingly independent ganglia that were bundled or juxtaposed together. The triganglia type had 3 seemingly independent ganglia that were aggregated together like a V or inverted-V shape. 5) The side-to-side symmetry of the DRG, in terms of signal intensity, location, or architecture symmetry of DRGs was determined.

The qualitative assessment, including the signal intensity, location, architecture, and symmetry were made by 2 experienced radiologists (J.S., J.Y.C.) in consensus. The quantitative measurement of dimensions was accomplished independently by 1 radiologist (J.S.).

Statistical Analysis

For overall analysis, descriptive statistics for the qualitative data were developed after pooling right and left sides, whereas the quantitative data of the ganglia dimensions were averaged across both sides. This procedure was to simplify the presentation of results. Side-to-side symmetry of the qualitative assessments was evaluated on paired (left and right) data by using the McNemar test.[11] For the quantitative measurements of ganglia diameters, paired *t* testing was used to assess side-to-side differences. Further comparison among different levels of the lumbar DRGs and between men and women was performed by using 1-way analysis of variance (ANOVA) and *t* test, respectively. The χ^2 test (when appropriate, the Fisher exact test) was used to analyze the distribution difference of qualitative assessments. All tests for statistical significance were performed for 2-tailed hypotheses with $P < 0.05$. Statistical calculations were done with SPSS Version 11.5 (SPSS for Windows, Chicago, Ill).

Results

All 1150 DRGs of bilateral spinal nerves from L1 to L5 in 115 volunteers (age range, 15–75 years; mean age, 40 years) were adequately visualized for the analysis both on the FFE images and on the reconstructed MIP images.

Positions of the DRGs

Almost all of the L1 through L3 DRGs were located in the foraminal or extraforaminal area (Table 1). All the L4 DRGs were located in the foraminal region. Of the 230 L5 DRGs, 217 (94.3%) were located in the foraminal region; 13 (5.7%) were in the intraspinal region. The intraspinal ganglia were found only at the L5 level ($P < .0001$). The incidence of intraspinal ganglia of DRG in women was higher than that in men, but there was no statistically significant difference ($P = .265$).

Table 1: Distribution of DRGs

	Intraspinal*	Foraminal	Extraforaminal	Total
L1				
Female	0 (0)	121 (99.2)	1 (0.8)	122
Male	0 (0)	108 (100)	0 (0)	108
Combined	0 (0)	229 (99.6)	1 (0.4)	230
L2				
Female	0 (0)	121 (99.2)	1 (0.8)	122
Male	0 (0)	107 (99.1)	1 (0.9)	108
Combined	0 (0)	228 (99.1)	2 (0.9)	230
L3				
Female	0 (0)	120 (98.4)	2 (1.6)	122
Male	0 (0)	105 (97.2)	3 (2.8)	108
Combined	0 (0)	225 (97.8)	5 (2.2)	230
L4				
Female	0 (0)	122 (100)	0 (0)	122
Male	0 (0)	108 (100)	0 (0)	108
Combined	0 (0)	230 (100)	0 (0)	230
L5				
Female	9 (7.4)†	113 (92.6)	0 (0)	122
Male	4 (3.7)†	104 (96.3)	0 (0)	108
Combined	13 (5.7)	217 (94.3)	0	230
Total	13	1129	8	1150

Note:—Data in parentheses are percentages calculated on the basis of the total of each sex. DRG indicates dorsal root ganglion.
* There was statistically significant difference in the distribution of DRG position among the different levels ($\chi^2 = 53.687$, $P < .0001$).
† At level L5, there was no statistical difference in the incidence of intraspinal ganglia of DRG between women and men (Fisher exact test, $P = .265$).

Signal Intensity of the DRGs

On the MIP images, 1113 (96.8%) DRGs demonstrated intermediate signal intensity (Fig 2); 37 (3.2%) DRGs were of high signal intensity, including 4 located at L5, 6 at L4, 8 at L3, 9 at L2, and 10 at L1, respectively. The incidence of DRG with high signal intensity increased progressively from L5 to L1, but there were no statistical differences among the L5 through L1 DRGs ($\chi^2 = 3.207$, $P = .524$).

Dimensions of the DRGs

The mean widths and lengths and width/length of the DRGs are shown in Table 2. The widths and lengths of the more caudad DRGs were statistically greater (ANOVA, $F = 200.984$, $P < .0001$; $F = 395.216$, $P < .0001$, respectively). The width/length ratio of the more caudad DRGs was statistically smaller except in L1 and L2 and L3 (ANOVA least significant difference test; L3 through L4; $P < .0001$; L4 though L5, $P < .0001$). The width and length of the L1 and L2 DRGs and the width of the L5 DRGs in men were statistically larger than those in women ($P < .05$). There was no statistical difference in remaining measured dimensions between women and men ($P = .189–0.884$).

Architecture of the DRGs

The numbers of singular ganglia, biganglia, and triganglia of each level DRGs are shown in Table 3. The distribution of ganglion architecture was statistically different among the different levels ($\chi^2 = 178.209$; $P < .0001$). The biganglia occurred more often in the L4 and L3 DRGs, whereas the singular ganglia more frequently occurred in the L5 and L2 DRGs, and especially the L1 DRGs (Fig 3). The triganglia could be occasionally found in the L5 through L2 DRGs, but not in the L1 DRGs (Fig 4). For the L4 DRGs, the incidence of bi- and triganglia of DRGs in women was statistically higher than that in men ($P = .043$).

Side-to-Side Symmetry of the DRGs

Symmetric ganglia position, signal intensity, and architecture of all 5 pairs of DRGs from L1 to L5 were found in 104 (90.4%), 96 (83.4%), and 30 (26.1%) subjects, respectively (Table 4). The right-left differences of all measurements were not statistically significant ($P > .05$); no tendency existed for 1 side to be complete more often than the contralateral side.

Discussion

The DRGs can be visualized by invasive imaging techniques such as myelography, epidurography, CT epidurography, CT diskography, radiculography, and preferably by noninvasive techniques such as MR imaging. Previously, radiologic studies revealed that the position of the DRGs is related to the occurrence of the variety and severity of radicular symptoms (pain and walking distance tolerance) in patients with extraforaminal lumbar disk herniation.[4,7-9,12] Most studies based on symptomatic patients or cadavers gave varying results on the morphology of the DRGs. Because the comparison between anatomic and clinical studies is somewhat problematic owing to the different conditions between cadavers and living human beings, the systemic survey of the DRG in the healthy population, especially with noninvasive techniques, is clinically significant. The study of 20 male volunteers with T1-weighted coronal MR imaging[10] provided precious information about the DRGs in healthy living subjects. However, because of the small number of subjects, singular sex distribution, and the narrow age range, the role of the study as normal baseline anatomic information of the DRGs is limited. In the present study, the DRGs of a healthy population with a wide age range were assessed. None of the subjects had symptoms. Thus, the morphometric information of the DRGs from this study could be used as a baseline anatomy to be compared with symptomatic patients.

In contrast to the invasive radiculogram or cross-sectional imaging, the 3D selective water excitation with Proset imaging in the present study could provide a full view of the DRGs. The Proset is another selective excitation technique to suppress either water or fat by exploiting the difference between water and fat resonance frequencies. The use of Proset does not additionally increase scanning time. With Proset, the signal intensity of fat was completely suppressed and the details of the DRGs were better delineated. To the best of our knowledge, this technique has not been reported in the evaluation of the DRGs. In our study, all the DRGs of bilateral spinal nerves from L1 to L5 were adequately visualized for the analysis on the MIP images. Occasionally, the ganglia were partially obscured by incompletely suppressed signals of the radicular vessels on the frontal coronal projection, whereas with the advantage of 3D imaging, the serial MIP images allowed easy discrimination of the ganglia from these vessels (Fig 5). This 3D imaging is superior to conventional coronal T1-weighted imaging and axial T2-weighted imaging. On the coronal T1-weighted imaging, 5 of 240 nerve roots could not be adequately visualized.[10] On the axial T2-weighted imaging, the DRGs were obliquely situated, so a serial observation was needed for accurate analysis.[8] With the ability of 3D visualiza-

Table 2: Dimensions of DRGs

	Level of DRG				
	L5	L4	L3	L2	L1
Width (mm)					
Female	6.22 ± 0.86	5.75 ± 0.84	5.25 ± 0.91	4.35 ± 0.88	3.23 ± 0.75
Male	6.60 ± 0.93	5.92 ± 1.03	5.49 ± 1.00	4.69 ± 0.86	3.55 ± 0.75
Combined	6.40 ± 0.91	5.83 ± 0.94	5.37 ± 0.96	4.51 ± 0.88	3.38 ± 0.77
P value*	0.025 (2.270)†	0.331 (0.975)	0.189 (1.323)	0.038 (2.099)†	0.026 (2.254)†
Length (mm)					
Female	11.55 ± 2.45	8.47 ± 1.45	7.05 ± 1.41	5.66 ± 1.03	4.14 ± 0.88
Male	11.61 ± 2.02	8.82 ± 1.52	7.36 ± 1.30	6.07 ± 1.17	4.58 ± 0.85
Combined	11.58 ± 2.25	8.64 ± 1.49	7.20 ± 1.36	5.85 ± 1.11	4.35 ± 0.89
P value*	0.884 (0.147)	0.200 (1.288)	0.222 (1.229)	0.044 (2.037)†	0.007 (2.749)†
Width/Length					
Female	0.28 ± 0.06	0.35 ± 0.05	0.38 ± 0.04	0.39 ± 0.04	0.39 ± 0.05
Male	0.29 ± 0.05	0.34 ± 0.06	0.37 ± 0.04	0.39 ± 0.04	0.39 ± 0.04
Combined	0.28 ± 0.05	0.34 ± 0.06	0.39 ± 0.04	0.39 ± 0.04	0.39 ± 0.05
P value*	0.225 (1.221)	0.630 (0.483)	0.739 (0.334)	0.565 (0.577)	0.601 (0.525)

Note:—Data are presented as mean ± SD. DRG indicates dorsal root ganglion.
* *t* test between women and men (*t* values in parentheses).
† The width and length of the L1 and L2 DRGs, and the width of the L5 DRGs differ statistically between men and women.

Table 3: Architecture of DRGs

	Singular	Biganglia	Triganglia	Total	*P* value
L1					
Female	119 (97.5)	3 (2.5)	0 (0)	122	0.058*
Male	100 (92.6)	8 (7.4)	0 (0)	108	
Combined	219 (95.2)	11 (4.8)	0 (0)	230	
L2					
Female	93 (76.3)	27 (22.1)	2 (1.6)	122	0.324 [2.254]†
Male	74 (68.5)	33 (30.6)	1 (0.9)	108	
Combined	167 (72.6)	60 (26.1)	3 (1.3)	230	
L3					
Female	66 (54.1)	56 (45.9)	0 (0)	122	0.34*
Male	61 (56.5)	45 (41.7)	2 (1.8)	108	
Combined	127 (55.2)	101 (43.9)	2 (0.9)	230	
L4					
Female	52 (42.7)	68 (55.7)	2 (1.6)	122	0.043*‡
Male	61 (56.5)	47 (43.5)	0 (0)	108	
Combined	113 (49.1)	115 (50.0)	2 (0.9)	230	
L5					
Female	101 (82.8)	18 (14.8)	3 (2.4)	122	0.453 [1.586]†
Male	95 (88.0)	12 (11.1)	1 (0.9)	108	
Combined	196 (85.2)	30 (13.0)	4 (1.8)	230	
Total	925	255	10	1150	

Note:—Data in parentheses and bracket are percentages calculated on the basis of the total of each sex and χ^2 values, respectively. DRG indicates dorsal root ganglion.
* Fisher exact text.
† Likelihood ratio test.
‡ The incidence of the bi- or triganglia differs statistically between female and male patients.

tion of DRGs, the dimensional measurements and architecture classification were, therefore, based on serial MIP images in our study.

Radiologically, the location of the DRG was classified into 3 types, and the incidence of the more proximally located DRG, so-called intraspinal type, increased as the level of the nerve root traveled down caudally.[7,8,10] In the present study, the intraspinal DRGs occurred merely at the L5 level with an incidence of 5.7%. The incidence of intraspinal DRGs at L5 is similar to that reported in the healthy young adults found on coronal T1-weighted imaging;[10] however, it is obviously lower than that in the symptomatic patients revealed by axial T2-weighted images.[8] This underlines again the observation that proximally located DRG is likely to be related to the clinical symptom. We also found that female volunteers had a slightly higher prevalence of intraspinal ganglia at L5. Nevertheless, like previous reports,[7,9] no cross-sex statistical difference was found. In the current study, almost all the DRGs manifested intermediate signal intensity on MIP images. For a given ganglion, a subtle higher intensity rim could be found. This may have resulted from the pattern of blood vessel distribution of the DRGs, which is characterized by a primarily internal arterialization with a superficial venous drainage.[13] In the present study, 3.2% of DRGs were of high signal intensity. That all the subjects were healthy without symptoms of low-back and radicular pain suggests that such high intensity could be a normal variant. The reason may be an unusually prominent or extensive perineural vascular plexus that obscures the relatively lower signal intensity of the

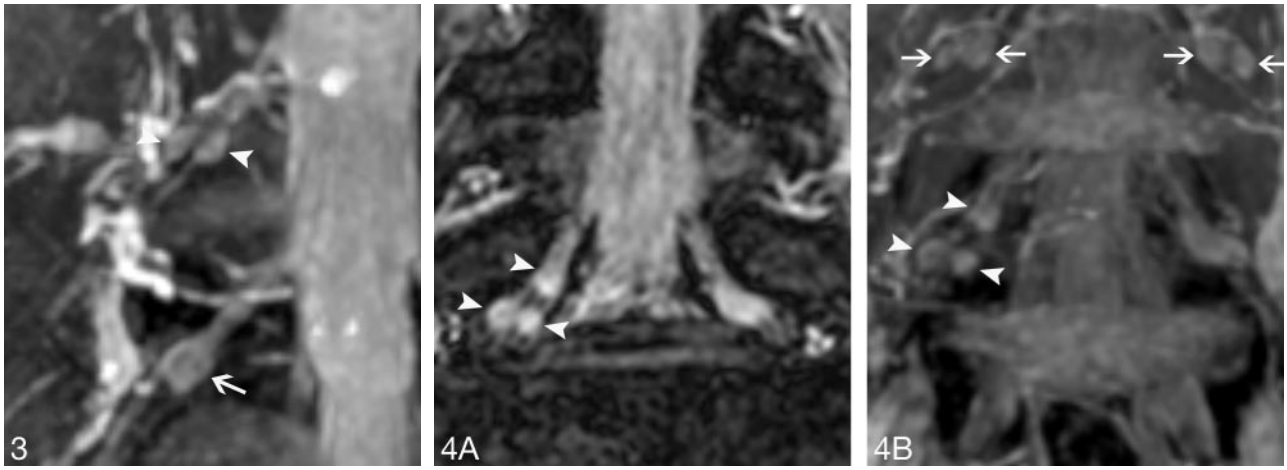

Fig 3. Architecture of DRGs. The singular right L5 DRG (*arrow*) and the biganglia right L4 DRG (*arrowheads*) are clearly demonstrated on the MIP image with an angle of 24° rotated to the right. The dimension of the DRGs on this plane is maximal, and the interference of adjacent vessels could be removed. Whether in biganglia or singular ganglion, a high intensity rim could be noted.

Fig 4. Triganglia architecture of L5. The right L5 DRG, with a composition of 3 separate ganglia, is defined as the triganglia.

A, The original FFE coronal image distinctly demonstrates the triganglia architecture of the right L5 DRG (*arrowheads*).

B, The MIP coronal image also clearly shows the triganglia architecture of the right L5 DRG (*arrowheads*). At same time, the biganglia architecture could be found in the L4 DRGs bilaterally (*arrows*).

Table 4: Symmetry of DRGs

	Level of DRGs				
	L1	L2	L3	L4	L5
Ganglia position*	NA	NA	1.000	NA	1.000
Signal intensity*	0.727	0.453	0.289	0.500	0.500
Width†	0.389 (0.865)	0.476 (0.716)	0.259 (1.134)	0.834 (0.210)	0.206 (1.271)
Length†	0.641 (0.467)	1.00 (0)	0.298 (1.044)	0.214 (1.250)	0.860 (0.176)
Width/Length†	0.610 (0.512)	0.339 (0.960)	0.751 (0.319)	0.639 (0.470)	0.332 (0.974)
Architecture*	0.453	0.065	0.435	0.876	0.407

Note:—Data are calculated *P* values. DRG indicates dorsal root ganglion.
* McNemar test. NA, the data is not applicable for the McNemar test because only 1, 2, and 0 pair DRGs are different in the position, respectively, at L1, L2, and L4 levels.
† Paired *t* test. Data in parentheses are *t* values.

nerve it surrounds, as observed by Williams et al.[14] However, this speculation should be verified by future histologic correlation.

In the current study, the dimensions of the DRGs varied according to the levels of nerve root. Both the widths and the lengths gradually increased as the DRGs were located more caudally. This finding is similar to the observation of Hasegawa et al[10] on the T1-weighted MR imaging, but in comparison with their results, the width and the length of the L5 DRGs in our study are both greater than their measurements. This difference may be caused by the use of different imaging techniques. Through the switching of serial-reconstructed MIP images with different angulations, we selected the radial plane on which the DRG could be maximally displayed to measure the dimensions. With conventional coronal images, it is difficult to demonstrate the full size of the L5 DRGs on a single section because of the more oblique and posterior course of the L5 nerve root across the neural foramen. Therefore, the real dimensions could be underestimated.

The cadaveric survey suggested that the DRGs are probably composed of 1 or 2 ganglia.[9] On the MIP images, we also observed this and thereby classified the DRGs into 3 types according to their composition. Moreover, the prevalence of each type varied according to different levels of nerve root, because the biganglia DRGs frequently occurred at the L4 (50.0%) and L3 (43.9%), whereas the singular ganglion often appeared at L5 (85.2%), L2(72.6%), and L1(95.2%). This radiologic classification had never been described previously and could only be correlated with the previous cadaveric study by Kickuchi et al,[9] who classified the bifurcated spinal nerve into 3 types: type A, type B, and type C, according to the connecting patterns of the DRGs. Comparatively, the singular ganglion in our study coincides with their types A and B DRGs, and the biganglia is consistent with type C. Furthermore, the incidence of type B DRGs at L5 and type C DRGs at L4 is essentially similar to our results. Notably, to our knowledge, the triganglia DRGs in this study have never been mentioned previously in either cadaveric or radiologic studies. The occasional occurrence of triganglia, we believe, is also an anatomic variant. More interesting, a cross-sex difference of the DRG architecture was found because the prevalence of bi- and triganglia of the L4 DRGs is higher in women than in men. Its potential role in the radiculopathy of different sexes is unclear.

Because the asymmetric findings may be pathologic, provided that scoliosis or malformation is not present, several authors specifically noted that the position asymmetry of

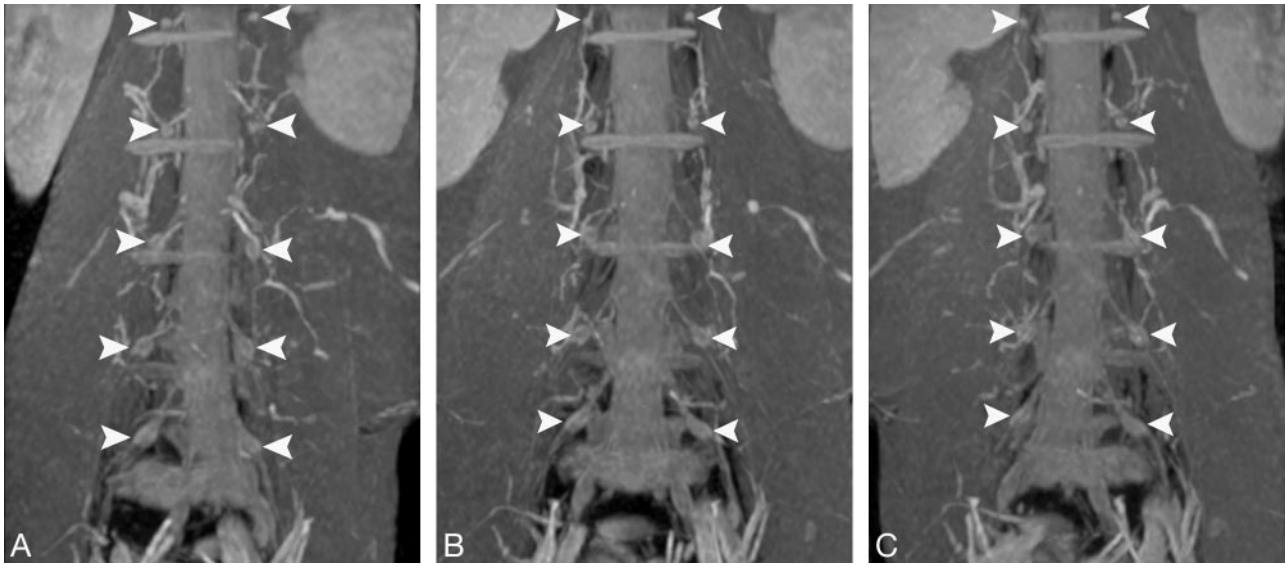

Fig 5. Lumbar DRGs on serial coronal MIP images. All 5 pairs of DRGs of the spinal nerves from L1 to L5 (*arrowheads*) are well displayed on serial views. Although some segmental and radicular vessels surrounding the DRGs are also displayed, the DRGs could be distinguished from these vessels by the rotation of the serial images with different angulations.

A, Left antero-oblique view.

B, Frontal view.

C, Right antero-oblique view.

DRGs could be caused by disk herniation or a degenerative hypertrophic facet in symptomatic patients.[7,8] In the present study, the ganglia position, dimension, signal intensity, and especially the architecture often differed from side to side for each pair of DRGs at all 5 levels from L1 to L5, but no tendency existed for 1 side to be complete more often than the contralateral side. Therefore, the asymmetric appearance of the DRGs should be carefully interpreted in the clinical practice because it may represent an anatomic variant.

This study has a limitation. An anatomic correlation was not feasible to prove the morphologic evaluation on MR imaging. With regard to a large number of healthy volunteers with a wide age range and a 3D visualization, our results could act as a radiologic baseline anatomy for lumbar DRGs in living humans.

Conclusion

The results of this study showed that the normal anatomy and variants of the lumbar DRGs could be clearly demonstrated by 3D FFE MR imaging with water selective excitation technique. The L5 DRGs are located most proximally. The sizes of the DRGs increase progressively from L1 to a maximum at L5. The relatively larger and more proximally located DRGs in the lower lumbar region may be more susceptible to compression than the upper DRGs. Some cross-sex morphologic differences also exist. An appreciation of normal anatomy and variants of the DRGs radiologically is important for the correct diagnosis of lumbosacral pain, for understanding pathologic anatomy in degenerative disorders, and for proper interventional or surgical treatment for radiculopathy.

References

1. Kobayashi S, Yoshizawa H, Yamada S. **Pathology of lumbar nerve root compression. Part 2. Morphological and immunohistochemical changes of dorsal root ganglion.** *J Orthop Res* 2004;22:180–88
2. Sugawara O, Atsuta Y, Iwahara T, et al. **The effects of mechanical compression and hypoxia on nerve root and dorsal root ganglia.** *Spine* 1996;21:2089–94
3. Vanderlinden RG. **Subarticular entrapment of the dorsal root ganglion as a cause of sciatic pain.** *Spine* 1984;9:19–22
4. Ohmori K, Kanamori M, Kawaguchi Y, et al. **Clinical features of extraforaminal lumbar disc herniation based on the radiographic location of the dorsal root ganglion.** *Spine* 2001;26:662–66
5. van Wijk RM, Geurts JW, Wynne HJ. **Long-lasting analgesic effect of radiofrequency treatment of the lumbosacral dorsal root ganglion.** *J Neurosurg* 2001; 94:227–31
6. Berger O, Dousset V, Delmer O, et al. **Evaluation of the efficacy of foraminal infusions of corticosteroids guided by computed tomography in the treatment of radicular pain by foraminal injection.** *J Radiol* 1999;80:917–25
7. Hasue M, Kunogi J, Konno S, et al. **Classification by position of dorsal root ganglion in the lumbosacral region.** *Spine* 1989;14:1261–64
8. Hamanishi C, Tanaka S. **Dorsal root ganglia in the lumbosacral region observed from the axial views of MRI.** *Spine* 1993;18:1753–56
9. Kikuchi S, Sato K, Konno S, et al. **Anatomic and radiographic study of dorsal root ganglia.** *Spine* 1994;19:6–11
10. Hasegawa T, Mikawa Y, Watanabe R, et al. **Morphometric analysis of the lumbosacral nerve roots and dorsal root ganglia by magnetic resonance imaging.** *Spine* 1996;21:1005–09
11. Agresti A. **Models for matched pairs.** In: Agresti A, ed. *Symmetry Models: Categorical Data Analysis*. New York: John Wiley & Sons; 1990:409–54
12. Cohen MS, Wall EJ, Brown RA, et al. **Cauda equina anatomy: II. Extrathecal nerve roots and dorsal root ganglia.** *Spine* 1990;15:1248–51
13. Parke WW, Whalen JL. **The vascular pattern of the human dorsal root ganglion and its probable bearing on a compartment syndrome.** *Spine* 2002;27: 347–52
14. Williams LS, Schmalfuss IM, Sistrom CL, et al. **MR Imaging of the trigeminal ganglion, nerve, and the perineural vascular plexus: normal appearance and variants with correlation to cadaver specimens.** *AJNR Am J Neuroradiol* 2003; 24:1317–23